Dynamics of ozone photoabsorption: A theoretical study of the Chappuis band

Antonio Banichevich, Sigrid D. Peyerimhoff, J. Alberto Beswick, and Osman Atabek

Citation: The Journal of Chemical Physics **96**, 6580 (1992); doi: 10.1063/1.462597
View online: http://dx.doi.org/10.1063/1.462597
View Table of Contents: http://scitation.aip.org/content/aip/journal/jcp/96/9?ver=pdfcov
Published by the AIP Publishing

Dynamics of ozone photoabsorption: A theoretical study of the Chappuis band

Antonio Banichevich and Sigrid D. Peyerimhoff
Institut für Physikalische und Theoretische Chemie, Universität Bonn, Wegelerstraße 12, D-5300 Bonn 1, Germany

J. Alberto Beswick
LURE,[a] Université de Paris Sud, F-91405 Orsay, France

Osman Atabek
Laboratoire de Photophysique Moléculaire,[b] Université de Paris Sud, F-91405 Orsay, France

(Received 12 March 1991; accepted 24 January 1992)

The first two excited singlet states of ozone are discussed in light of recent *ab initio* MRD-CI calculations. In the asymmetric pathway for $O_2 + O$ fragmentation, the two $1\,^1A_2$ and $1\,^1B_1$ states undergo an avoided crossing resulting in the $C\,^1A''$ and $D\,^1A''$ states. The $D\,^1A''$ state has bound vibrational levels in the Franck–Condon region while the $C\,^1A''$ is repulsive (towards $O_2 + O$ fragmentation) in that area and is found to possess a local minimum away from the Franck–Condon area at small bond angles. A one-dimensional cut along the dissociation reaction coordinate was extracted from the three-dimensional calculated potential surfaces. Quantum mechanical calculations of the absorption spectrum based on these one-dimensional *ab initio* potentials and of the corresponding *ab initio* transition moments were undertaken. The present work assigns the distinct features of the Chappuis band to the bound levels of the $D\,^1A''$ state superimposed on the $C\,^1A''$ state continuum as an alternative interpretation of the second absorption band in the ozone spectrum.

I. INTRODUCTION

The predissociative nature of ozone represents an important key in atmospheric chemistry.[1–3] In particular, photofragmentation of O_3 resulting from solar light absorption in the wavelengths of the Huggins and Hartley bands has received considerable attention because of its implication for atmospheric uv shielding. The visible absorption (Chappuis band[4–6] has also been studied, both experimentally[7–10] and theoretically.[9] Finally, experimental near-infrared absorption (Wulf band[11,12]) has been reported only recently.[13] Because of the small stability of this molecule a satisfactory interpretation of its absorption spectrum requires that, not only the Franck–Condon area, but also the possible fragmentation channels to be considered. Under these considerations, ozone provides a particularly interesting model system for the detailed study of state-to-state photodissociation dynamics. Since the molecule is highly symmetrical, it also provides two energetically equivalent fragmentation channels which may lead (as in other AB_2 systems[14,15]) to interference effects and trapped trajectories, and therefore to structures and oscillations in the otherwise smooth photodissociation continuum.

Since ozone is made up of only three light atoms, theoretical calculations, including both *ab intio* determination of the relevant potential energy surfaces as well as dynamical simulation of the fragmentation, are possible. In the present work we thus study the visible absorption region of ozone (Chappuis band) and its significance for the photoprocess

$$O_3(X\,^1A_1) + h\nu \xrightarrow{400<\lambda<650\ \text{nm}} O(^3P_g) + O_2(X\,^3\Sigma_g^-) \qquad (1)$$

by quantum mechanical methods, using previously calculated *ab initio* potential energy surfaces.[16] The Chappuis absorption band is known to consist of a bell-shaped continuum extending from 430 to 750 nm (13 330 to 23 260 cm^{-1}) with its maximum between 597.5 and 602.5 nm ($\sim$16 000–16 740 cm^{-1}),[3,8,12,17] plus a series of peaks superimposed on the blue side of the spectrum. The observed band spacing is between 800 and 1300 cm^{-1}.[12] This higher-energy structure suggests the existence of a bound state. Furthermore, in this band almost no temperature dependence of the absorption cross sections is found.[17] In a previous theoretical work,[9] a single excited electronic state ($1\,^1B_1$ in C_{2v} symmetry) was invoked and the discrete features superimposed to the background continuum were assigned to symmetric stretch vibrations perpendicular to the dissociation coordinate.

The new *ab initio* calculations performed for this study show that there are actually two potential surfaces in the energy region of the Chappuis band which can absorb from the ground electronic state $X\,^1A_1$ if the restriction of C_{2v} symmetry is not maintained. The first, labeled $C\,^1A''$ in the lower C_s symmetry is repulsive with respect to the dissociation coordinate and very similar in character to the one considered in previous work.[9] The second, labeled $D\,^1A''$ possesses a potential minimum in the energy range of the

[a] Laboratoire du CNRS, CEA et MEN.
[b] Laboratoire du CNRS.

 0021-9606/92/096580-11$06.00

lower-energy side of the maximum in this absorption band. Both states are linear combinations of the $1\,^1A_2$ and $1\,^1B_1$ states in C_{2v} symmetry, and their potential surfaces result from an avoided crossing in the lower C_s symmetry. Such behavior has also been discussed in the photodissociation dynamics of H_2S in the 195 nm band.[18,19] Since the two surfaces are very close in energy in the Franck–Condon region, the structures seen in the Chappuis band could very well be due to the bound levels of the $D\,^1A''$ electronic state. In addition, the two surfaces can couple by nonadiabatic interactions, and this could partly be responsible for the observed widths.

In the present work we will make use of some of the *ab initio* results for these two electronic states, while later work will be devoted to the discussion of more details. Calculations for the dynamics will be carried out for both electronic states considering the dissociation reaction coordinate R_2. The potential curves for the two states maintaining C_{2v} symmetry will also be discussed in comparison with earlier work for completeness.

II. POTENTIAL SURFACE CALCULATIONS

The oxygen functions are taken from the Dunning $(9s,5p)$ basis set in the $(5s,3p)$ contraction.[20] One diffuse s, one diffuse p, and one d polarization function with exponents 0.15, 0.05, and 1.2, respectively, were added so that our standard basis can be described as a contracted $(6s,4p,1d)$ set. In addition, one s and one p bond-type Gaussian with exponents $\alpha_s = 1.15$ and $\alpha_p = 0.90$, respectively,[6,21] were located between each pair of the oxygen atoms. The AO basis employed for the calculations in C_{2v} symmetry thus consists of 84 contracted Cartesian Gaussians (CCG1). For the calculations in C_s symmetry the p bond-type functions are deleted, which gives an AO basis set of 75 contracted Cartesian Gaussians (CCG2).[16]

The configuration interaction treatment is the standard multireference single and double excitation (MRD-CI) procedure.[22,23] For the CI calculations 18 electrons were correlated leaving a core of the three doubly occupied $1s$ oxygen orbitals. A selection of configurations is done for the final secular equation, while the energy is extrapolated to the eigenvalue of the entire space of generated MRD-CI configurations using a perturbation technique.[6,22,23]

The potential surfaces corresponding to the variation of all three internal coordinates have been calculated. In the symmetric arrangement of nuclei (C_{2v} symmetry) the ozone bond lengths ($R_1 = R_2 = R$) are varied between 2.20 and 3.0 a_0, and the bond angle γ between 40° and 180°. The asymmetric ozone structure was calculated at the three bond angles $\gamma = 100°$, 116.8°, and 133.6°, while values for the bond lengths were chosen as $2.0a_0 \leqslant R_1 \leqslant 2.8a_0$ and $2.0a_0 \leqslant R_2 \leqslant 10\,a_0$.

A. Symmetric arrangement of nuclei: C_{2v} symmetry

Using a single determinant the electronic configuration of the O_3 molecule in its ground state is given in C_{2v} notation by

$$\cdots(5a_1)^2(3b_2)^2(1b_1)^2(6a_1)^2(4b_2)^2(1a_2)^2. \qquad (2)$$

The total SCF energy obtained in the CCG1 basis for the ground state at its equilibrium geometry $\gamma = 116.8°$ and $R_1 = R_2 = R = 2.413\,a_0$ is $E_{SCF} = -224.327\,33$ hartree.

For the configuration interaction calculations the SCF MO's of the $X\,^1A_1$ state are chosen. In addition, a basis of natural orbitals is employed where the transformation from SCF MO's to the natural orbitals (NO) is accomplished by carrying out an MRD-CI calculation for the $1\,^3B_1$ electronic state at larger configuration selection thresholds ($T = 30\times10^{-6}$ hartree), followed by diagonalization of the resultant first-order density matrix. The motivation and details of this treatment will be discussed in a forthcoming paper.[24]

The technical details for the various calculations of the singlet states considered for the first two $O_2 + O$ dissociation channels are indicated in Table I. It is seen that the total number of generated configuration state functions is on the order of two million; only between 8 500 and 10 900 among these were treated explicitly in the secular equations, whereas the contribution of the remaining species was estimated in the standard MRD-CI manner. The number of reference configurations was between 13 and 19.

The potential energy surfaces are obtained by employ-

TABLE I. Results and technical details for the singlet states considered for the O_3 molecule at the equilibrium geometry $R_1 = R_2 = 2.413\,a_0$ and $\sphericalangle OOO = 116.8°$ employing the basis CCG1.[a]

State	$xMyR$	Number of total SAF's	SAF's selected	Vertical energy (in eV) E_{MRD-CI}	$E_{est.\ FCI}$	C^2
$X\,^1A_1$	$19M2R$	2 246 601	10 926	0.0 ($-224.976\,56$ a.u.)	0.0 ($-225.026\,64$ a.u.)	91.00%
$1\,^1B_1$	$16M2R$	2 543 942	8 603	2.205	2.100	91.00%
$1\,^1A_2$	$13M2R$	1 863 794	9 096	2.213	2.160	90.00%

[a] Given are the number of reference of main configurations (xM) and the number of roots (yR) according to which configuration selection is carried out, the total number of symmetry-adapted configuration state functions (SAF's) which have been generated and the largest selected subspace at the threshold energy of 2.0×10^{-5} hartree which has been diagonalized explicitly. Since the calculations are carried out in the C_{2v} subgroup, the irreducible representation correlation is indicated in the first column. The last column gives the contributions of the reference space to the total MRD-CI expansion. CI values based on NO's.

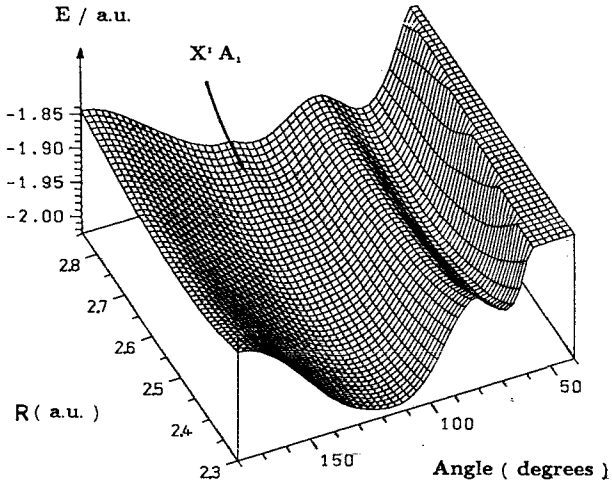

FIG. 1. Potential energy surface for the ground state $X\,^1A_1$ as function of the angle γ and O–O bond length (R) in C_{2v} symmetry. The estimate full CI energy is given as $E_{\text{Full-CI}} = -223.0 + E$ in a.u.

ing the two-dimensional set of grid points. The results for the ground and excited states are shown in Figs. 1 and 2(a). The characterization of these states as obtained from the two-dimensional (R,γ) potential surface are contained in Tables II and III. The second minimum of the ground state near 60° will be discussed elsewhere.[24] The crossing between the two excited C_{2v} states is best seen from Fig. 2(b), which shows the respective angular curves at optimized internuclear separation R.

Considering the lowest fragmentation channel $O(^3P_g) + O_2(^3\Sigma_g^-)$, the electronic states $X\,^1A_1$ and the excited states $1\,^1A_2$ and $1\,^1B_1$ as function of the angle and O–O_2 separation are of interest. It is seen that the calculated ground state potential surface reproduces the characteristic spectroscopic parameters, i.e., geometry and fundamental frequencies, very well (Table III). It should be noted, however, that the harmonic approximation for the two-dimensional potentials is employed in evaluating the frequencies. The agreement for the excited states is somewhat worse, but given the harmonic approximation[24] and the complexity of the actual states on one hand, and the simple adiabatic treatment in only C_{2v} symmetry on the other, the deviations between calculated frequencies and those derived from measurements are certainly not surprising.

Important for the present consideration are the excited states. The vertical excitation energies classify the $1\,^1B_1$ state as the lowest excited singlet with a vertical energy of 2.10 eV above the ground state. If the potential minima are considered instead, this $1\,^1B_1$ state is the second excited singlet lying 1.82 eV above the absolute minimum of the ozone ground state. The equilibrium geometry for this state is found at $R = 2.55\ a_0$ and $\gamma = 117.2°$, which is close to the

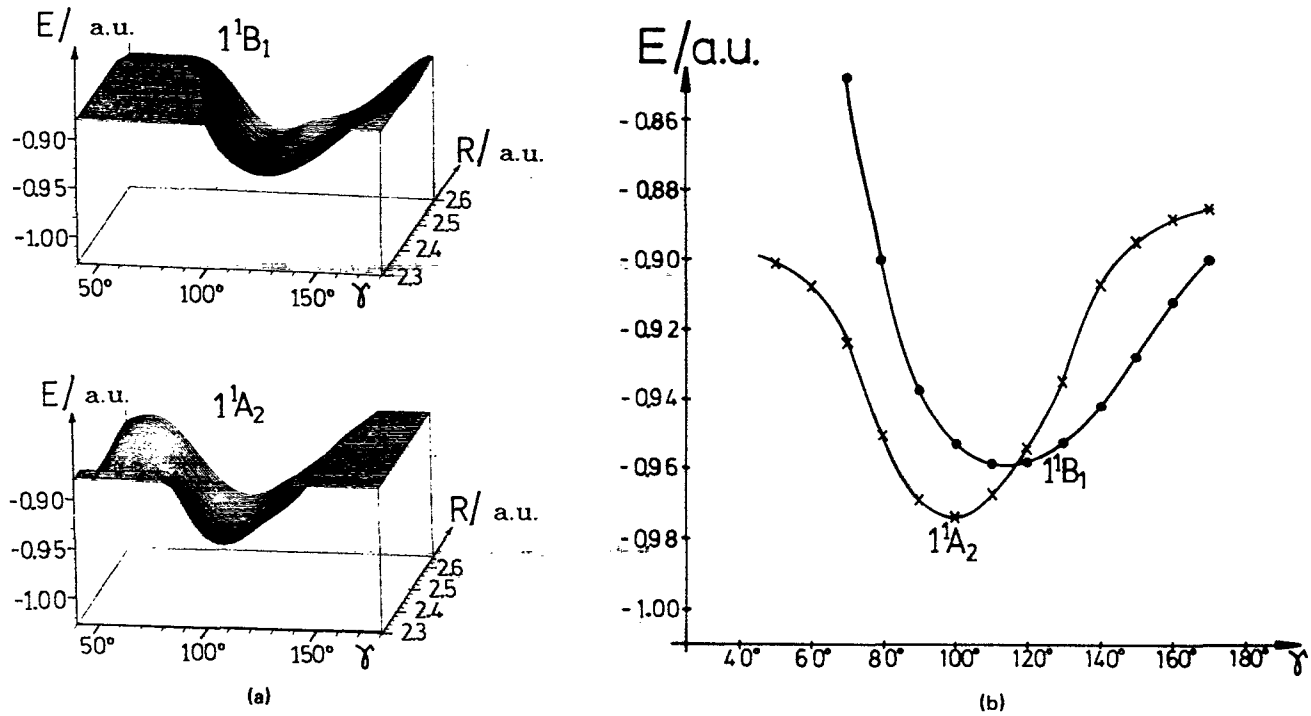

FIG. 2. (a) Potential energy surfaces for the excited $1\,^1B_1$ and $1\,^1A_2$ electronic states as function of the angle γ and O–O bond length (R) in the C_{2v} symmetry. The estimate full CI energy is given as $E_{\text{Full-CI}} = -224.0 + E$ in a.u. (b) Potential energy curves at optimized R values as a function of the internuclear angle for the two excited $1\,^1B_1$ and $1\,^1A_2$ states showing the crossing of states.

TABLE II. Summary of the calculated geometries and adiabatic energy values between potential minima energies in O_3 compared with previous results; $R = R_1 = R_2$ is given in a_0 and $\sphericalangle OOO = \gamma$ in degrees.

State	Vertical energy[a] $E_{est.\ FCI}$	Values from spline fit[a,b] Adiabatic	Geometry R	Geometry γ	Previous studies (Ref. 25)[a,c] Adiabatic	Geometry R	Geometry γ
$X\,^1A_1$	0.0	0.0	2.43	116.0	0.0	2.45	116.0
	(− 225.026 64)	(− 225.027 00)			(− 224.610 25)		
$1\,^1B_1$	2.10	1.82	2.55	117.2	2.06	2.59	117.7
$1\,^1A_2$	2.16	1.44	2.54	100.0	1.66	2.60	100.7

[a] The present vertical and adiabatical energies are given in eV; the absolute energies (in parentheses) are given in hartree.
[b] The spline fit values are obtain from the two-dimensional minimization of the energy surface.
[c] The absolute energy is taken from the used POL-CI-R method (Ref. 25).

values of 2.59 a_0 and 117.7° given in earlier *ab initio* work.[25] Hence the present work finds a bond length which is about 5% longer than that of the ground state but nearly the same equilibrium angle. The calculated vertical transition moment is $\mu_{XB} = 1.50 \times 10^{-2}$ a.u., and thus characterizes the transitions from the ground state to this state as the second strongest of the allowed lower-energy transitions in ozone.[24] The zero-point energy for the symmetric bending mode indicates a relatively flat potential surface compared to the symmetrical stretching.

The other electronic state in the same energetic region is $1\,^1A_2$ with a vertical energy of 2.16 eV; transitions to this state from $X\,^1A_1$ are formally forbidden according to the C_{2v} selection rules. Its minimum is found 1.44 eV above the ground state minimum (Table II) and thus this state should be considered the lowest excited singlet state of O_3. This is in agreement with earlier *ab initio* work,[25] which calculated the minima of both excited states considered here to be about 0.2 eV higher. Measurements[13] deduce the lowest minimum at 1.304 eV. The equilibrium geometry for $1\,^1A_2$ is found for $R = 2.54\ a_0$ and $\gamma = 100°$, and again shows a bond length elongation of about 5% relative to the ground state, just as in the $1\,^1B_1$ state, but contrary to the latter, a considerable reduction in the bond angle by about 14% compared to $X\,^1A_1$. The calculated fundamental frequencies (Table III) show similar characteristics as for the $1\,^1B_1$ state.

In previous work[13] the $1\,^1A_2 \leftarrow X\,^1A_1$ absorption has been modeled as a vibronically allowed $1\,^1A_2$ $(v_1', v_2', v_3' = 1) \leftarrow X\,^1A_1\,(v_1, v_2, v_3 = 0)$ transition, where the asymmetrical stretch activity weakens the C_{2v} selection rule. The experimental results confirm the proposed temperature dependence of the absorption[12] and indicate a small value for ν_3' of about $90 \pm 80\ cm^{-1}$,[13] thereby suggesting that the absorber state is unbound with respect to asymmetric motions.

Since the $O + O_2$ dissociation limit is at 1.13 eV,[28,29] the minima of both states, as obtained in C_{2v} symmetry, lie above the dissociation channel. On the other hand, dissociation is unlikely to occur by maintaining C_{2v} symmetry. Hence the potential surfaces in the asymmetric O_2–O nuclear conformation (C_s symmetry) are of great importance. Both states, $1\,^1B_1$ and $1\,^1A_2$ belong to the same $^1A''$ irreducible representation in this symmetry, and the crossing of surfaces, as seen in Figs. 2(b) and 3(a), turns into an avoided crossing as indicated in Figs. 3(b) and 3(c). This avoided crossing occurs in the Franck–Condon area $(R, 110° \leqslant \gamma \leqslant 120°)$[24] and is seen to happen near 117° along the R-optimized energy pathway as a function of the internuclear angle [Fig. 2(b)].

B. The asymmetric O_2–O distortion: C_s symmetry

Using the same single determinant for the electronic configuration [Eq. (2)] but using the CCG2 basis set, the total SCF energy for the ground state at its equilibrium geometry is $E_{SCF} = -224.318\,72$ hartree. Considering a slight asymmetrical deformation of the equilibrium geometry, the electronic configuration of the ozone ground state in C_s symmetry becomes

$$\cdots (7a')^2 (8a')^2 (1a'')^2 (9a')^2 (10a')^2 (2a'')^2. \qquad (3)$$

TABLE III. Comparison of calculated (MRD-CI) and experimental zero-point frequencies in O_3; values of a previous work are also included. All values are given in cm^{-1}. (ν_1 is symmetric stretch, ν_2 is bending)

State	Present work ν_1	Present work ν_2	Values from Ref. 25 ν_1	Values from Ref. 25 ν_2	Experiment ν_1	Experiment ν_2	Reference
$X\,^1A_1$	1105.0	706.0	1235.0	704.0	1110.0	705.0	28
	...	...	...	...	1103.0	701.0	26
	...	...	...	...	1134.9	716.0	27
$1\,^1B_1$	1091.0	476.0	965.0	489.0	930.0	460.0	9
$1\,^1A_2$	1093.0	675.0	1160.0	537.0	...	566.7	12
	...	...	...	...	~1200.0	528.0	13

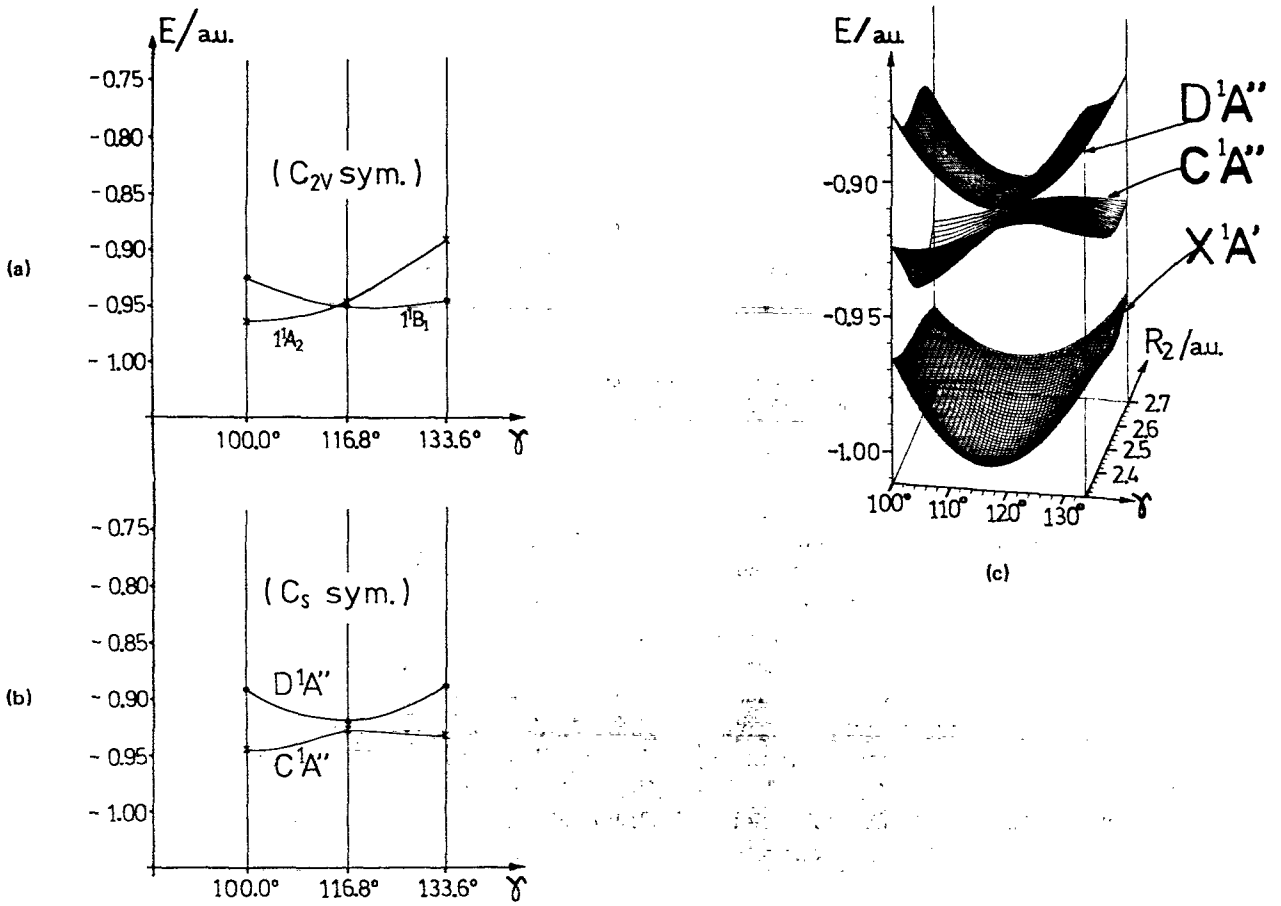

FIG. 3. Schematic representation of states considered under different symmetry considerations as a function of internuclear angle: (a) Potential energy surface cut at $R = 2.413\,a_0$ in C_{2v} symmetry with the crossing between $1\,^1B_1$ and $1\,^1A_1$ electronic states; (b) Potential energy surface cut at $R_1 = R_2 = 2.413\,a_0$ in C_s symmetry with the $C\,^1A''$ and $D\,^1A''$ electronic states as a result of the avoided crossing; (c) Potential energy surface as function of the dissociation coordinate R_2 in the C_s symmetry with ground state $X\,^1A_1$ and the $C\,^1A''$ and $D\,^1A''$ electronic states with $R_1 = 2.413\,a_0$. For all three representations the estimate full-CI energy is given as $E_{\text{Full-CI}} = -224.0 + E$ in a.u.

The actual calculated energy is $E_{\text{SCF}} = -224.318\,93$ hartree.

For the configuration interaction calculations the SCF MO's of the $^5A'$ state are chosen. Details concerning this choice and further results will be discussed elsewhere.[30]

For the C_s potential energy surfaces the three-dimensional set of grid points was $2.00a_0 \leqslant R_1 \leqslant 2.8a_0$, $2.00a_0 \leqslant R_2 \leqslant 10.0\ a_0$ at three representative angles $\gamma = 100.0°$, 116.8°, and 133.2°, (i.e., $\pm 20\%$ of the equilibrium angle). An optimization of the surface as a function of angle was not undertaken. In previous work the characterization of the different electronic states based on a two-dimensional consideration of the energy surfaces is given.[16] Table IV contains a summary of the results. The calculated values as seen from the vertical energies deviate somewhat from the values obtained in C_{2v} symmetry (Table I) at the same nuclear geometry. Compared to the C_{2v} treatment the AO basis set is slightly different, but more importantly the CI basis functions (here $^5A'$ MO's, previously NO's) as well as the MRD-CI treatment, which is primarily designed to describe the O_2–O dissociation, differ from the procedure in Sec. II A. Hence these deviations on the order of 0.2–0.3 eV should be considered as within the error margins. Note also the similarity to earlier *ab initio* work[25] which also shows higher values (Table II).

In the present context it is important to consider the angle variation as outlined in Fig. 3(b). An avoided crossing of the parent states $^1A_2$ and $^1B_2$ leads to the states $C\,^1A''$ and $D\,^1A''$ which correlate with different dissociation channels, i.e., $C\,^1A''$ with $O(^3P_g) + O_2(^3\Sigma_g^-)$, and the other $D\,^1A''$ with the higher channel $O(^1D_g) + O_2(^1\Delta_g)$. Such avoided crossing is also important for triplet states[24] giving rise to a repulsive and a metastable ozone triplet potential surface. The two-dimensional potential surfaces corresponding to the stretching of both O–O bond lengths (R_1 or R_2) for the $C\,^1A''$ and $D\,^1A''$ electronic states of ozone are presented in Figs. 4(a) and 4(b) at the fixed angle 116.8°, respectively. They show the following characteristics.

At small angles the $C\,^1A''$ possesses a local minimum [Fig. 3(b) and Fig. 3(c)] around 1.44 eV or lower (Table II), and a barrier exists towards O_2–O dissociation in the R_2 coordinate [Fig. 3(c)]. In the Franck–Condon region of the

TABLE IV. Some results and technical details[a] for the singlet states considered for O_3 employing CCG2. The technical data are at the equilibrium geometry $R_1 = R_2 = 2.413\ a_0$ und $\sphericalangle OOO = 116.8°$.

State	$xM\ yR$	Number of total SAF's	SAF's selected	Vertical ($E_{est.\ FCI}$)	Minimum[b] (in eV)
$X\,^1A'$	$48M\,4R$	7 180 526	16 724	0.0 ($-225.011\,44$ a.u.)	0.0
$C\,^1A''$	$44M\,3R$	7 292 251	12 826	2.41	...
$D\,^1A''$	$44M\,3R$	7 292 251	12 826	2.64	2.10

[a] Given are the number of reference of main configurations (xM) and the number of roots (yR) according to which configuration selection is carried out, the total number of symmetry-adapted configuration state functions (SAF's) which have been generated and the largest selected subspace at the threshold energy of 2.0×10^{-5} hartree which has been diagonalized explicitly. The weight of the reference configurations in the final wave function was larger than 89% for all three states and internuclear separations R_2. Since the calculations are carried out in the C_s subgroup, the irreducible representation correlation is indicated in the first column. Only the ground state $X\,^1A'$ can be directly assigned C_{2v} symmetry. The $^5A'$ SCF-MO's are employed in the CI.

[b] The theoretical values are derived from two-dimensional spline fit surfaces in (R_1,R_2). Optimization in the angle was not considered.

ground state [Fig. 4(a)], i.e., at higher energies (around 2.41 eV, Table IV), this state shows a purely repulsive O_2–O potential surface. In other words, this state is expected to be metastable with a local potential minimum at angles smaller than 117°. The transition $C\,^1A'' \leftarrow X\,^1A'$ is allowed according to C_s selection rules, the calculated transition moment μ_{CX} close to the Franck–Condon area is in the order of 10^{-2} a.u. [Fig. 5(a)]. Experimental studies of the Wulf bands[13] indicate that the lifetime of the upper state decreases rapidly with increasing vibrational quanta and observe a progression which can be assigned up to $v_3' \leqslant 1$. It is thus very likely that this $C\,^1A''$ (i.e., for angles smaller than 117° it is $1\,^1A_2$) state must be assigned to the carrier of the Wulf bands (bending motion), as has already been assumed in the comparison of experimental and calculated data in Table III.

The second state, $D\,^1A''$ exhibits a potential minimum with respect to angular as well as stretching deformations [Fig. 3(c) and Fig. 4(b)]. Its minimum energy in the disso-

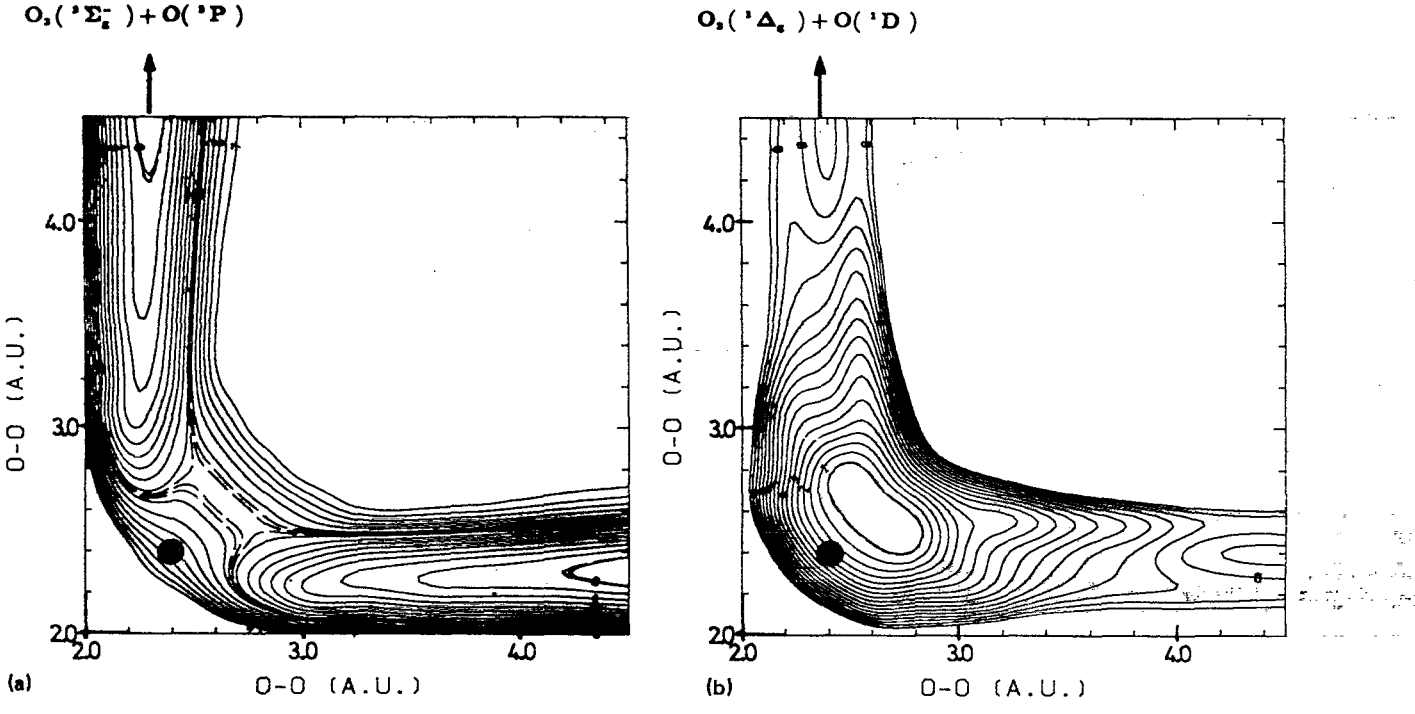

FIG. 4. Two-dimensional potential energy surface as a function of R_1 and R_2 (O–O bond elongation) at $\gamma = 116.8°$. The difference between two contour lines is 1000 cm^{-1} (0.124 eV): (a) $C\,^1A''$ state; (b) $D\,^1A''$ state.

ciation surface is 2.10 eV above the ground state at $R_1 = R_2 = 2.56\,a_0$ for an assumed angle of 116.8°,[16] which leads to a calculated dissociation energy of 1.8 eV into the $O_2(^1\Delta_g) + O(^1D_g)$ fragments. If all geometrical parameters are optimized, the absolute minimum is expected to be somewhat lower; as seen from Table II it is 1.82 eV in the different MRD-CI treatment for the symmetric structure. The transition moment μ_{DX} [Fig. 5(b)] is of similar magnitude as for the C state.

In Table V the results for the asymmetric stretching modes of the $X\,^1A'$ and $D\,^1A''$ states obtained in the calculations in which the optimized bond angle values are employed, are summarized. In these calculations the two-dimensional potential surfaces in (R_1,R_2) have been considered in the harmonic approximation as done previously. For both bound electronic states $X\,^1A'$ and $D\,^1A''$ it can be seen that the symmetric and the antisymmetric[16] stretching frequencies are roughly equal.

The vertical energy gap between the two interacting states $C\,^1A''$ and $D\,^1A''$ for $R_1 = 2.413$ a.u. (0.23 eV) is larger than the corresponding energy difference (0.06 eV) between $1\,^1B_1$ and $1\,^1A_2$ (Table II) in the C_{2v} restricted calculation. This is in line with the general behavior of interacting states (in particular, conical intersections), although not too much weight should be placed on the actual number because of the errors (a few tenths of an eV) inherent in the various theoretical treatments.

III. THE ABSORPTION CROSS SECTION FOR THE CHAPPUIS BAND

A. Description of model

In the wavelength region $\lambda = [400,650]$ nm (Fig. 6) the ozone molecule shows a discrete structure in the absorption spectrum. In addition, a prompt fragmentation of ozone in the lowest channel $O_2\ (X\,^3\Sigma_g^-) + O(^3P_g)$ after absorption has been observed for this photoexcitation experimentally.[9,37] Considering the experimental data,[3,8,9,12,17,37] we note that the interpretation of this absorption band is based solely on the single state $1\,^1B_1$–$X\,^1A_1$ transition, i.e., the presence of the $1\,^1A_2$ state has been so far entirely neglected. Due to its repulsive character in the O–O bond length elongation in the Franck–Condon region ($C\,^1A''$) and its coupling with the $1\,^1B_1$ state at lower symmetry (C_s), a considerable lowering of the intensity for transitions to the lowest-lying vibrational levels v_1' and v_2' of the $1\,^1B_1$ state [see Fig. 2(b)] is expected. Another consequence of this coupling to the continuum should be a broadening of the lowest vibrational levels for the (v_1',v_2') progressions.

Analysis of the structures observed in the Chappuis absorption band carried out by Levene *et al.*[9] indicates vibrational frequencies of $\nu_1 = 930$ and $\nu_2 = 460\ \text{cm}^{-1}$ (Table III). More precisely, the authors were able to assign vibrational progressions for the $1\,^1B_1 \leftarrow X\,^1A_1$ transition progressions in a range of 160 nm by taking v_1' and $v_2' = 0,1$ to correspond to (harmonic) symmetric stretching and bending modes, respectively. They note very little optical activity in the bending progression, and a short progression in the symmetric stretch. The maximum transition amplitude corresponds to the first excited level of the symmetric stretch and the zero-point level of the bending. In addition, the vibrational frequencies of the surface considered were calculated as 965 and 489 cm^{-1} (Ref. 9), in good agreement with the observations. Therefore, the observed peaks in the spectra were assigned to bound–bound transitions for those vibrations which are orthogonal to the reaction coordinate.

Taking into account the actual form of the present potential surfaces in question, we investigated the photoabsorption process (1) in the framework of a model which considers the electronic states $C\,^1A''$ and $D\,^1A''$ resulting from conical intersection. As discussed previously, both states possess different characters in the Franck–Condon region, and two ways can be pursued for the theoretical description of the Chappuis absorption band.

First, for the description of the discrete structure, i.e., the vibrational progression in this band, for which the treatment of the problem is appropriate in terms of the C_{2v} symmetry internal coordinates defined as

TABLE V. Summary of the calculated geometries (R_1,R_2,γ) and adiabatic energy values relative to the ground state minimum and corresponding frequencies of O_3. Distances in a_0, energies in eV, and frequencies in cm^{-1}.

{Symmetry}		Geometry $(R_1R_2\gamma)$		Excitation energy			ν_3[a]		
C_{2v}	C_s	Experiment	Present work	Vertical	Minimum[b]	Experiment[c]	Absorption band	Experiment	Present work
$X\,^1A_1$	$\rightarrow X\,^1A'$	(2.413,2.413,116.8)[d]	(2.41,2.41,116.6)	0.0	0.0	0.0	⋯	1089	1104
								1042	
$1\,^1B_1$	$C\,^1A''$	⋯	(⋯,⋯,~100.0)[e]	2.41	<1.44	1.24–1.65	Wulf	⋯	⋯
$1\,^1A_2$	$D\,^1A''$	⋯	(2.56,2.56,~116.0)[f]	2.64	<2.10	1.65–2.88	Chappuis	⋯	1073

[a] Normal stretching mode ν_3. The experimental values for the zero-point frequency are taken from Refs. 26, 27, and 28, respectively.
[b] The theoretical values are derived from two-dimensional spline fit surfaces in (R_1,R_2); the dependence on the internuclear angle γ has been taken into account.
[c] The experimental limits for the absorption bands has been taken from the measured spectra. See Refs. 4, 8, 11–13, 17, 31–36.
[d] From Ref. 28.
[e] This electronic state possesses a local minimum at smaller angles than 110° with a barrier towards R_2 dissociation of ~0.53 eV (Ref. 24).
[f] In the Franck–Condon region a unique correlation between excited C_{2v} and C_s states is not possible due to the avoided crossing, but close to the minimum of the $D\,^1A''$ state this state would correlate with $1\,^1B_1$ (see also Table II).

$$S_1(A_1) = \frac{1}{\sqrt{2}}(R_1 + R_2),$$
$$S_2(A_1) = \gamma, \tag{4}$$
$$S_3(B_2) = \frac{1}{\sqrt{2}} = (R_1 - R_2).$$

Because both bound states $X\,^1A'(X\,^1A_1)$ and $D\,^1A''(1\,^1B_1)$ have symmetric equilibrium geometries at similar angles (Tables II and V), the dipole allowed absorption process $D\,^1A''(1\,^1B_1) \leftarrow X\,^1A'$ can be described with this set of coordinates. The $C\,^1A''(1\,^1A_2) \leftarrow X\,^1A'$ transition does not contribute to the discrete structure of the spectrum for $\lambda = [400,650]$ nm.

Second, if the photofragmentation in the Chappuis band is also of interest, as in the present work, the behavior of the potential along the asymmetrical ozone distortion is also of importance. Taking into account that experimentally the fragmentation (1) has been observed[8,9,37] as net result of the photoexcitation, the total width of the Chappuis absorption band should be described by considering the fragmentation limit for the $O_2 + O$ bond breaking, i.e., the continuum. In order to include this into the absorption band a new set of coordinates has been chosen, i.e., an adequate set of internal coordinates for the description of a repulsive state in Franck–Condon region which dissociates in $O_2(^3\Sigma_g^-) + O(^3P_g)$:

(1) The bond length of the "diatomic" O–O fragment of the molecule R_1 is kept constant (2.413 a_0).

(2) The elongation of the other O–O length, R_2 which approximately corresponds to the reaction coordinate of a photodissociative process is considered. For large values of R_2, this coordinate system becomes the Jacobi system usually employed in atom–diatomic scattering.

(3) The angle γ between R_1 and R_2 is held at 116.8°, i.e., the equilibrium angle for both bound electronic states, $X\,^1A'$ and $D\,^1A''$ $(1\,^1B_1)$ (see Tables II and V).

This set of coordinates represents an effective one-dimensional model with a simple O–O bond length playing the role of the reaction coordinate, whereby the other two vibrational degrees of freedom are represented by relatively steep potential profiles being orthogonal to the reaction coordinate. It is, of course, possible, at least in principle, to use the C_{2v} symmetry internal coordinates to describe the repulsive state, but because of the strong coupling of S_1 and S_3 in the area away from the Franck–Condon region such an approach would require much greater computational expenditure, in particular, also a large portion of the potential hypersurface[28] (O–O–O elongation).

The ν_1 and ν_3 vibrational frequencies of both bound states $X\,^1A'$ and $D\,^1A''$ are found to be very similar to one another (see Tables III and V). This means that the frequency corresponding to the stretching of one of the O–O bonds (calculated in an effective one-dimensional approximation by using the corresponding diagonal element of the kinetic energy matrix) has also practically the same value in both states. Furthermore, only the S_1 coordinate is effectively active in the absorption process $1\,^1B_1(v_1' = 0, v_2' = 0, v_3' = 0) \leftarrow X\,^1A_1(v_1 = 0, v_2 = 0, v_3 = 0)$. This enables a reliable representation of the vibrational transitions in terms of a single O–O bond length coordinate R_2. Taking these two findings into account, we consider the discrete structure for the transition $D\,^1A''$ $(1\,^1B_1) \leftarrow X\,^1A'$, in the photodynamical calculations to arise from the quantum number v', which is essentially equivalent to v_1' (S_1).

B. Photodynamical calculations

We have performed absorption line shape calculations for ozone excited with photon wavelengths between 400 and 750 nm. The transition dipole moments μ_{CX} and μ_{DX} employed are those of Figs. 5(a) and 5(b), respectively. It should be noted, because of the fact that one of the A'' states treated correlates with the $1\,^1A_2$ specie in the C_{2v} geometry ($R_1 = R_2 = 2.413$ a.u.), the corresponding transition moment function should vanish at this point. However, since the adiabatic potential surfaces calculated in the C_s symmetry show a sharp avoided crossing [see Fig. 3(a) at $R_1 = R_2$) with the consequence that the corresponding wave functions are of mixed B_1 and A_2 character, both of the transition moments μ_{CX} and μ_{DX} are computed to be different from zero, and, moreover, to be of similar magnitude at $R_1 = R_2$. A proper C_{2v}-symmetry behavior can be obtained by transforming the computed electronic wave functions for the corresponding C and D states into their diabatic counterparts.[38]

The following dynamical approximations have been made:

(1) The rotational and vibrational motions are independent of one another.

(2) As the initial state we choose the zero-point level of the electronic ground state.

(3) The electronic state C is considered only as an absorber without any coupling to the D state.

(4) A width has been given to each of the D state vibrational levels v' accounting for instrumental (and collisional) and predissociation broadening. Its value was taken as an adjustable parameter.

Using these approximations the absorption cross section is evaluated as the sum of two independent contributions from the C and the D states. The cross section for absorption of a photon with energy $E = h\nu$ (where $\nu = c/\lambda$ from the initial state $|\Phi_0^{(X)}\rangle$ with total energy zero, is then given by

$$\sigma_{\mathrm{TOTAL}}(\lambda) = \sigma^{(C)}(\lambda) + \sigma^{(D)}(\lambda) \tag{5}$$

with

$$\sigma^{(C)}(\lambda) = \frac{8\pi^3}{\lambda} |\langle \chi_E^{(C)} | \mu_{cx} | \chi_0^{(X)} \rangle|^2 \tag{6}$$

and

$$\sigma^{(D)}(\lambda) = \sum_{v'} |\langle \chi_{v'}^{(D)} | \mu_{DX} | \chi_0^{(X)} \rangle|^2 \frac{\Gamma_{v'}/2}{(\mathrm{hc}/\lambda - E_{v'})^2 + \Gamma_{v'}^2/4}, \tag{7}$$

where μ_{CX} and μ_{DX} are the transition dipole moments, and $|\chi_E^{(C)}\rangle$ is the final continuum wave function (with total energy $E = \mathrm{hc}/\lambda$) correlating asymptotically (i.e., for $R_2 \to \infty$) to $O_2(^3\Sigma_g) + O(^3P_g)$, while $|\chi_v^{(D)}\rangle$ is a vibrational bound

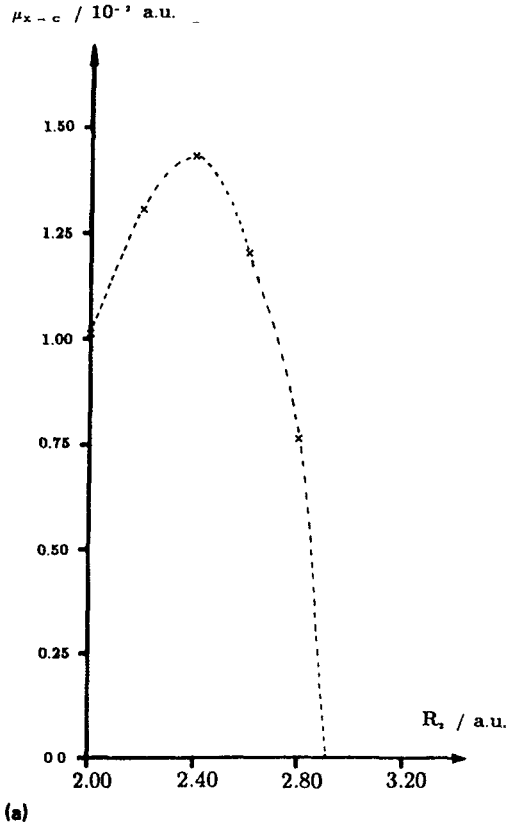

FIG. 5. Calculated transition moments for the two excited electronic states (a) $C\,^1A''$ and (b) $D\,^1A''$ at $\gamma = 116.8°$ and $R_1 = 2.413\,a_0$ as a function of R_2.

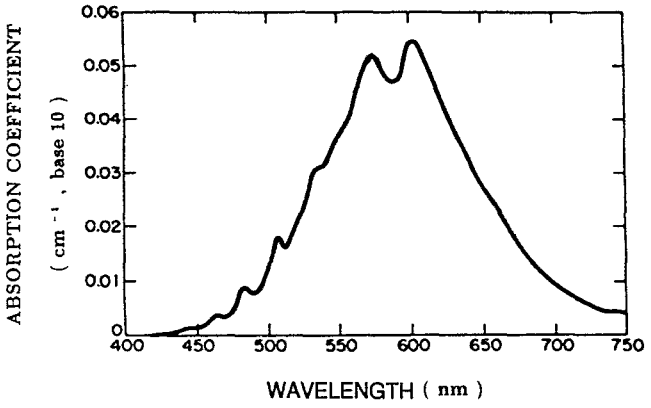

FIG. 6. The ozone Chappuis absorption spectrum from Ref. 32.

wave function of the D state with total energy $E_{v'}$. Finally, $\Gamma_{v'}$ is the phenomenological width associated to the $\chi_{v'}^{(D)}$ levels and $E_{v'}$, their energy. The $|\chi_0^{(X)}\rangle$ vibrational wave function has been obtained by Numerov integration of

$$\left[-\frac{\hbar^2}{2m}\frac{\partial^2}{\partial R_2^2} + V_x(R_2)\right]\chi_0^{(X)}(R_2) = E_0\chi_0^{(X)}(R_2) \qquad (8)$$

with m being the reduced mass for the relative motion of the fragments, which in our case is two-thirds of the oxygen atom mass. The same technique was used for the calculation of the $|\chi_E^{(C)}\rangle$ and $|\chi_{v'}^{(D)}\rangle$ wave functions. For the continuum wave function, $|\chi_E^{(C)}\rangle$, the following energy-normalized asymptotic condition is used

$$|\chi_E^{(C)}\rangle = \sqrt{\frac{2m}{\pi\hbar^2 k}}\cos(kR_2 + \varphi), \qquad (9)$$

where $k = \sqrt{2m[E - V_C(\infty)]}/\hbar$.

C. Results and discussion

The calculated absorption cross sections, considering only the upper C state are shown in Fig. 7. The results which are obtained are similar to those of Levene *et al.*:[9]

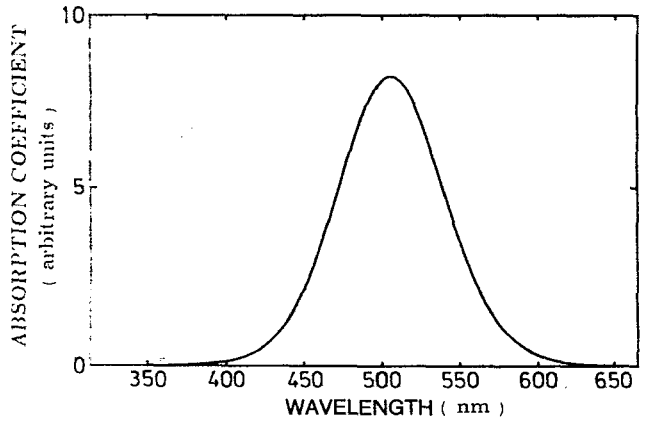

FIG. 7. Calculated absorption spectrum only for the $C\,^1A''$ electronic state. See the text for explanation.

(i) The line shape is nearly symmetric;
(ii) the width at half-maximum is equal to 81 nm, significantly narrower than the experimental value (129 nm);
(iii) the maximum of the spectrum is at 506 nm (2.45 eV) shifted with respect to the experiment by 0.41 eV to the blue.

Figure 8 displays the results including C and D for $\Gamma_{v'} = 550\ \text{cm}^{-1}$. Several changes with respect to the C-only spectrum are observed:

(i) The line shape is now asymmetric with a sharper rise for short wavelengths;
(ii) the width at half-maximum slightly increases to 85 nm;
(iii) the maximum is now at 515 nm (2.40 eV);
(iv) more important perhaps is the appearance of structures in the blue wing of the band.

It is obvious that this spectrum closely resembles the experimental one. In particular, it shows now structures superimposed on to the background continuum. The spacing between the first six peaks is given around 970 to 1045 cm^{-1}. In Table VI we present the calculated energies and the integrated intensities

$$I_{v'} = |\langle \chi_{v'}^{(D)} | \mu_{DX} | \chi_0^{(X)} \rangle|^2 \tag{10}$$

of the $X \rightarrow D$ vibrational transitions. Three comments are in order.

First, the two peaks appearing at the maximum of the spectrum correspond to bound–bound transitions to the $v' = 2$ and 3 vibrational levels of the D state. The peaks associated to the $v' = 0$ and $v' = 1$ levels, which would appear on the red wing of the band, are not seen due to their very small intensities. The fact that the maximum intensity for the bound–bound transitions occurs for $v' = 2$–4, is due to the shift of the D potential curve by 0.29 a_0 towards larger internuclear distances with respect to the ground state, and also to the strong dependence on distance of the transition dipole in the Franck–Condon region [see Fig. 5(b)]. Measured absorption cross sections of the Chappuis in condensed phase[10] show some vibronic features at the low-energy side of the band with increasing intensity at 626, 648, and 697 nm. The most prominent vibronic features are at 597 and 575 nm, however, and correspond to the gas phase at 607 and 574.5 nm,[9] respectively. The weak transitions are apparently enhanced in the perturbing environment and have therefore not been seen in the gas phase; they would support the present theoretical interpretation according to which additional features corresponding either to transitions to the lowest-lying vibrational levels of the electronic bound D state, or to possible bound levels of the "perturbed" repulsive C state could be expected.

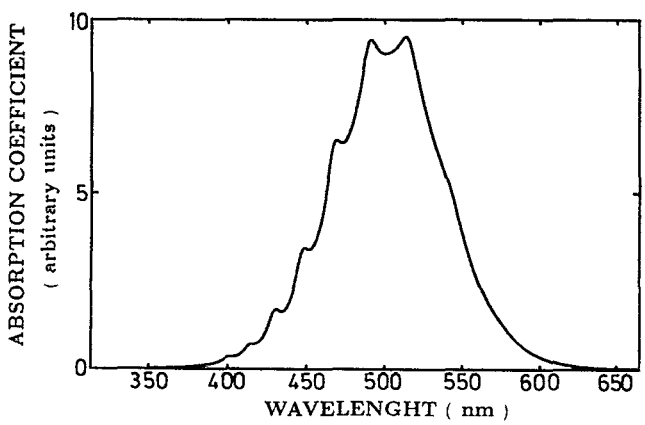

FIG. 8. Calculated absorption spectrum considered for the two $C\,^1A''$ and $D\,^1A''$ electronic states. See the text for explanation.

TABLE VI. Energies and integrated intensities for the bound–bound transitions $D(v') \leftarrow X(v = 0)$.

v'	$\lambda_{v'}$ (nm)	$I_{v'}$[a] (a.u.)
0	575.0	1.2×E-6
1	542.4	7.0×E-6
2	514.9	2.0×E-5
3	489.9	2.4×E-5
4	467.3	2.4×E-5
5	447.1	1.5×E-5
6	429.2	9.0×E-6
7	413.6	3.0×E-6
8	399.9	1.5×E-6

[a] The notation 1.0×E-5 stands for 1.0×10^{-5}.

Second, the main differences between the calculated and the experimental spectra are the position of the band and its width. The shift of 0.36 eV can be due to an overall energy displacement of the *ab initio* excited curves with respect to the ground level. As for the width, there are several possible causes which can be invoked. Slight changes in the slope of the potential for the C state in the Franck–Condon region are known to modify the width, and the contribution of the other degrees of freedom (bending and rotation as well as vibration) to the dynamics should be taken into account. Also, finite temperature and the population of many initially excited rotational levels of the molecule may influence the width of the absorption spectrum considerably. In addition, we have not considered the absolute minimum of the D state with 2.10 eV at $R_1 = 2.56\ a_0$, but the pathway with R_1 kept fixed at 2.413 a_0 whose minimum is found at $R_2 = 2.70\ a_0$ with 2.18 eV.

Finally, the known experimental limit of the Chappuis band is around $\lambda = 430$ nm (2.88 eV). Between this limit and the beginning of the Huggins band at 360 nm (3.44 eV)[33–35] with marked temperature dependence,[8,10,33–36] we expect structural features, but of very low intensity, on the basis of our present calculations. In this energy range a predissociative behavior for the photofragmentation [Eq. (1)] of the electronic D state is assumed. The increase in the Huggins band intensity for $\lambda \leqslant 360$ nm is due to another electronic state dissociating into the $O_2 + O$ ground state fragments, which has not been considered here. In the present work the potentials have been taken from the *ab initio* calculations and no attempt to fit the experimental spectrum has been made.

IV. CONCLUSIONS

We have presented *ab initio* MRD-CI calculations for the ground state and the first two excited singlet states of ozone. In most theoretical discussions only symmetric variations in bond lengths and bond angles have been considered so far, predicting two close-lying states of $1\,^1A_2$ and $1\,^1B_1$ symmetry, in which the observed absorption in the visible region has been attributed to the second of these since $X\,^1A_1$–$1\,^1A_2$ intercombinations are not allowed according to the dipole-selection rules in C_{2v} symmetry. As soon as antisymmetric distortions occur, as expected for the O_2–O dissociation, both states can interact in the lower C_s symmetry, and their potential surfaces show an avoided crossing close to the Franck–Condon region of the ground state. Absorption is possible for both states, labeled $C\,^1A''$ and $D\,^1A''$.

The first absorption spectrum, the Wulf bands, is assigned to the metastable $C\,^1A''$ electronic state possessing a local minimum around 100°. The temperature behavior of this band is consistent with our interpretation.

The one-dimensional quantum calculation for the absorption spectrum of ozone based on the $C\,^1A''$ and $D\,^1A''$ *ab initio* potentials with an effective one-dimensional model, i.e., the dissociation coordinate R_2 as degree of freedom, and calculated electronic transition moments suggest a new interpretation for the width and discrete features in the Chappuis absorption spectrum: the repulsive $C\,^1A''$ state potential absorbs, yielding the width of the band, and prompting dissociation into the translationally hot, ground electronic state fragments, $O_2 + O$; the discrete features are assigned to absorption by the bound vibrational levels of the second potential surface ($D\,^1A''$ state), which lies in the same energy region as $C\,^1A''$. The calculated absorption pattern models the measured spectrum quite successfully. It is furthermore found that at wavelengths $\lambda \leqslant 607$ nm, additional structures with relatively low intensity should be present in the Chappuis continuum.

Since there is no experimental evidence for emission in the energy region of $\lambda = [430,750]$ nm, it can be speculated that for higher energies in the blue wing of the Chappuis absorption band, the $D\,^1A''$ state predissociates via nonadiabatic coupling with the $C\,^1A''$ state. Experimental investigation for photofragment energy partitioning distribution of $O_2 + O$ and vibrationally–rotationally spectra of the diatomic fragment produced by photodissociation of O_3 at wavelengths between 500 and 360 nm would be of importance to confirm this, since these two states correlate with different fragment channels. Obviously the present consideration cannot discriminate between different interpretations and a full 3D treatment is necessary to settle this question.

Note added in proof. In a parallel treatment M. Braunstein *et al.*[39] considered the corresponding counterparts of the $X\,^1A_1$, $1\,^1A_2$, and $1\,^1B_1$ states for the open form ($R \leqslant 2.80a_0$, $90° \leqslant \gamma \leqslant 130°$) and for the region about the cyclic form ($R \leqslant 2.90a_0$, $59.5° \leqslant \gamma \leqslant 60.5°$) of ozone in C_s symmetry. Their results are in good agreement with the present work for the calculated spectroscopic parameters (equilibrium geometry and vibrational frequencies ν_1 and ν_2) and for the energies of the electronic excited states in the Franck–Condon region.

ACKNOWLEDGMENTS

The authors wish to thank Dr. Octario Roncero and Dr. Miljenko Perić for many helpful discussions. We thank the Deutsche Forschungsgemeinschaft (Leibniz-Prize) and the CNRS for financial support given to part of this work. The services and computer time made available by the University of Bonn Computer Center and CIRCE (Orsay) have been essential to the present study and are gratefully acknowledged.

[1] H. Okabe, in *Photochemistry of Small Molecules* (Wiley, New York, 1976).
[2] R. P. Wayne, Atmos. Environ. **21**, 1683 (1987).
[3] Global Ozone Research and Monitoring Project Report No. 16, *Atmospheric Ozone* (World Meteorological Organization, Geneva, 1985).
[4] J. Chappuis, C. R. Acad. Sci. (Paris) **91**, 985 (1880); **94**, 858 (1882).
[5] P. J. Hay and W. A. Goddard III, Chem. Phys. Lett. **14**, 46 (1972).
[6] K. H. Thunemann, S. D. Peyerimhoff, and R. J. Buenker, J. Mol. Spectrosc. **70**, 432 (1978).
[7] P. W. Fairchild and E. K. C. Lee, Chem. Phys. Lett. **60**, 36 (1978).
[8] J. I. Steinfeld, S. M. Adler Golden, and I. M. Gallagher, J. Phys. Chem. Ref. Data **16**, 911 (1987).
[9] H. B. Levene, J. C. Nieh, and J. J. Valentini, J. Chem. Phys. **87**, 2583 (1987).
[10] V. Vaida, D. J. Donaldson, S. J. Strickler, L. Stephens, and J. W. Birks, J. Phys. Chem. **93**, 506 (1989).
[11] C. R. Lefebvre, Acad. Sci. (Paris) **200**, 1743 (1935).
[12] O. R. Wulf, Proc. Natl. Acad. Sci. **16**, 507 (1930).
[13] S. M. Anderson, J. Morton, and K. Mauersberger, J. Chem. Phys. **93**, 3826 (1990).
[14] O. Atabek, M. T. Bourgeois, and M. Jacon, J. Phys. Chem. **87**, 5870 (1987).
[15] M. Jacon, O. Atabek, and C. Leforestier, J. Chem. Phys. **91** 1585 (1989).
[16] A. Banichevich, S. D. Peyerimhoff, and F. Grein, Chem. Phys. Lett. **173**, 1 (1990).
[17] E. Vigroux, Ann. Phys. (Paris) **8**, 709 (1953).
[18] K. Weide, V. Staemmler, and R. Schinke, J. Chem. Phys. **93**, 861 (1990).
[19] R. N. Dixon, C. C. Marston, and G. G. Balint-Kurti, J. Chem. Phys. **93**, 6520 (1990).
[20] T. H. Dunning, Jr., J. Chem. Phys. **53**, 2823 (1970).
[21] S. D. Peyerimhoff and R. J. Buenker, J. Chem. Phys. **47**, 1953 (1967).
[22] R. J. Buenker and S. D. Peyerimhoff, Theoret. Chim. Acta **39**, 217 (1975).
[23] R. J. Buenker, S. D. Peyerimhoff, and W. Butscher, Mol. Phys. **35**, 771 (1978).
[24] A. Banichevich and S. D. Peyerimhoff (in preparation).
[25] P. J. Hay and T. H. Dunning, J. Chem. Phys. **67**, 2290 (1977).
[26] D. J. McCaa and J. H. Shaw, J. Mol. Spectrosc. **25**, 374 (1968).
[27] A. Barbe, C. Secroun, and P. Jouve, J. Mol. Spectrosc. **49**, 171 (1974).
[28] G. Herzberg, in *Electronic Spectra and Electronic Structure of Polyatomic Molecules* (Van Nostrand, Princeton, 1966).
[29] G. Herzberg, in *Spectra of Diatomic Molecules* (Van Nostrand, Princeton, 1950).
[30] A. Banichevich, S. D. Peyerimhoff, and F. Grein (in preparation).
[31] I. Tanaka, E. C. Y. Inn, and K. Watanabe, J. Phys. Chem. **21**, 1651 (1953).
[32] E. C. Y. Inn and Y. Tanaka, J. Opt. Soc. Am. **43**, 870 (1953).
[33] J. C. D. Brand, K. J. Cross, and A. R. Roy, Can. J. Phys. **56**, 327 (1978).
[34] D. H. Katayama, J. Chem. Phys. **71**, 815 (1979).
[35] D. E. Freeman, K. Yoshino, J. R. Esmond, and W. H. Parkinson, Planet. Space Sci. **32**, 239 (1984).
[36] A. Sinha, D. Imre, J. H. Goble, and J. L. Kinsey, J. Chem. Phys. **84**, 6108 (1986).
[37] D. S. Moore, D. S. Bomse, and J. J. Valentini, J. Chem. Phys. **79**, 1745 (1983).
[38] F. T. Smith, Phys. Rev. **179**, 111 (1969).
[39] M. Braunstein, P. J. Hay, R. L. Martin, and R. T Pack, J. Chem. Phys. **95**, 8239 (1991).